Bulletin of the Mineral Research and Exploration

http://bulletin.mta.gov.tr

Estimation of co-seismic land deformation due to Mw 7.3 2017 earthquake in Iran (12 November 2017) using Sentinel-1 DInSAR

Fatma CANASLAN ÇOMUT[a*], Şule GÜRBOĞA[b] and Tayeb SMAIL[c]

[a]*Disaster and Emergency Directorate of Denizli (AFAD Denizli), Turkey,*
[b]*General Directorate of Mineral Research and Exploration, Turkey*
[c]*Department of Civil Engineering, Blida University, Algeria*

Research Article

Keywords:
Interferometry, DInSAR, 12 November 2017 Iran earthquake.

ABSTRACT

A strong shaking with Mw 7.3 occurred on 12th November 2017 around the Sarpol-e Zahab town in the border area between Iran and Iraq. It has a number of foreshocks and aftershocks increasing the total deformation, cumulatively. In this study, we have investigated how earth surface deformed after such a strong earthquake and its scatters. Because, the deformation inspection are indispensable for the safety of citizens and infrastructures. The best way for monitoring of surface deformation in such a big event is the SAR technique. This system can work effectively during night and day under different weather conditions. The Interferometric SAR (InSAR) allows accurate measurements of surface deformation in mm resolution. There are several methods for the application of SAR techniques and one of them is Differential InSAR (DInSAR) indicating an uplift and subsidence around epicentral area precisely. We preferred to use it for sensitive vertical displacement in the target area. The seismological data from the observatory centers indicate that the recent earthquake sourced from the NW-SE trending, northeast dipping High Zagros Reverse Fault Zone. According to the results, epicentral area has been exposed a vertical displacement with 90 cm uplift and -41 cm subsidence in the northeastern and southwestern block of the fault, respectively.

Received Date: 26.12.2018
Accepted Date: 01.07.2019

1. Introduction

Sarpol-e Zahab earthquake is the largest event after the occurrence of 1909 earthquake around the shaking area (Ambraseys and Melville, 1982). 1909 and recent events sourced from the Zagros fold belt in the Zagros vicinity that has the most of the active faults of Iran. The reason for the seismic activities in this region is the continental collision between the African-Arabian and Eurasian plates (Şengör and Kidd, 1979; Dewey et al., 1986; Dilek et al., 2009; Ghalamghash et al., 2016; Fahim Guilany et al., 2019) (Figure 1). Moreover, the Zagros fold belt is characterized by a folded 12–14 km thick sedimentary cover deposited on the northeastern continental border of the Arabian plate (Falcon, 1974; Colman-Sadd, 1978). From early Mesozoic to Quaternary, the collision creates a compressional tectonic regime where compression has stemmed from subduction of NeoTethyan oceanic crust underneath the Iranian Central Block, and the subsequent collision between the Arabian and Eurasian plates along the Zagros suture zone (Şengör and Kidd, 1979; Dewey et al., 1986; Dilek et al., 2009; Ghalamghash et al., 2016). Naturally, the area experiences the high seismic activity. The convergent motion creates a huge amount of relief differences and elevated mountainous area.

Citation info: Canaslan Çomut, F., Gürboğa, Ş., Smail, T. 2020. Estimation of co-seismic land deformation due to Mw 7.3 2017 earthquake in Iran (12 November 2017) using Sentinel-1 DInSAR. Bulletin of the Mineral Research and Exploration 162, 11-30. https://doi.org/10.19111/bulletinofmre.604026

* *Corresponding author: Fatma CANALAN ÇOMUT, fatma.c.comut@afad.gov.tr*

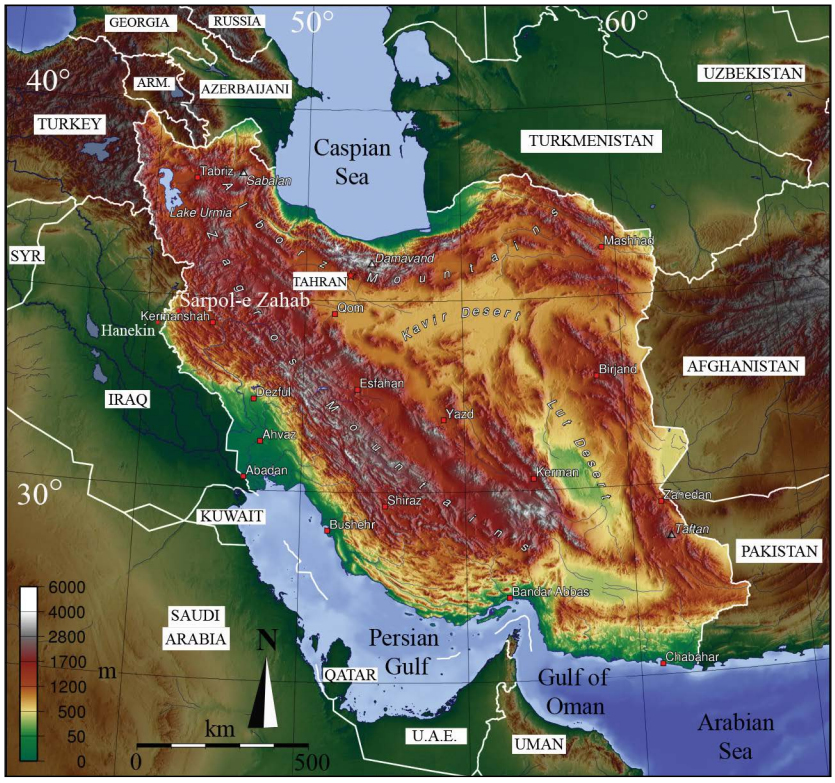

Figure 1- Map of Zagros area showing the location of Sarpol-e Zahab and Hanekin settlements with digital elevation model of the area (Emami et al., 2010).

Comparing two towns in both sides of mountainous area and plateau area of the fold belt, Sarpol-e Zahab is located 618 m in the Iran, and Hanekin is located 200 m above the sea level in the Iraq (Figure 1, Emami et al., 2010). There is approximately 400 km altitude difference in just 50 km distance between these towns. In case of such a big earthquake, an important vertical displacement should be happening and the amount of vertical motion is significant for the deformation in the crust. Newly growing technologies give a chance to determine vertical displacement in cm to mm scale.

Satellite Interferometric Synthetic Aperture Radar (InSAR) is a technique being develop very intensively during last 20 years (Hanssen, 2001). It is famous for giving information about vertical ground motion or deformation of structures in a millimetric scale. When it is compared with the older systems achieving the detection of surface deformation, there are many advantages and disadvantages. One of the advantage is related to high spatial resolution and short temporal range between the measurements. It means the same area is being monitored with high resolution in a more frequent time slices. It will increase the sensitivity of the taken data. On the other hand, the signal could be often lost due to the weather condition, agricultural activity etc. In this case, it could not be possible a solution for the lost data. However, this problem is tried to be solved with improved satellite technologies.

Within new satellite systems of high revisit time as Sentinel-1/2, InSAR has now a huge capacity to provide more reliable and useful information that can be used to offer detection of hazardous movements at the surface, their delineation and spatiotemporal description. This can be applied in practice as within an early warning system to avoid the damages such as identification of slow landslide motions, determination of sinkholes or static risk evaluation for buildings and structures. An approach of detecting risk for infrastructure using InSAR is currently in experimental stage, however the potential is discussed and proved by several works (Thiebes, 2012; Intrieri et al., 2013). The technique that would semi-automatically process a long time series of high quality satellite SAR image. It is used for the recognition of recent movements in a selected area using different approaches such as Permanent Scatterers (Ferretti et al., 2005). This method can be

extended by probabilistic approach in order to provide an estimation of structural deformation in near future, supposing a continuous trend of detected movement. Detected and predicted movements of a structure or earth surface can be evaluated with other data such as geological settings or reference in-situ measurements that would cause a risk of serious damages. A proper interpretation could be applied with an interdisciplinary connection of other experts offering a completeness of the system.

This paper presents a transfer of knowledge about InSAR technology and methodological aspects of InSAR application towards detection of dangerous terrain and structure movements due to Mw 7.3, 12 November 2017 Iran earthquake. We focus on estimating the co-seismic displacements along the line-of-sight LOS direction by mean of interferometry SAR. In order to investigate this issue, we used Interferometric Synthetic Aperture Radar. Presented results are based on the processing of SAR data using Differential InSAR, to highlight the benefits of high resolution SAR sensors for the purpose of deformation monitoring, the datasets are from Sentinel-1 SAR images with 2 different passes, ascending and descending. The main objectives for this work is to detect ground LOS displacement, for the earthquake that struck Iraq-Iran border on 12 November 2017 and its effect on nearby villages.

2. Methodology

Interferometric Synthetic Aperture Radar (InSAR) is a microwave imaging system and belong the system SAR signals contains amplitude and phase components of the same pixel. With this technology it is possible to measure surface movement and estimate the topography (Pritchard, 2006; Kim, 2013). SAR imaging uses amplitude (intensity) of backscattered echoes. Radar sees through clouds – all – weather imagining is possible and doesn't need illumination by the Sun – can image day and night. Surface roughness and slopes control the strength of the backscatter. All full resolution SAR images have both an amplitude component and a phase component; called as "SLC (single look complex)".

The multiplication of master SLC data and a conjugate of slave SLC data generates an interferogram which includes topographic phase effect, atmospheric distortion, baseline errors and noise (Kim, 2013; Netzband et al., 2007; Goudarzi 2010). The calculation of interferogram is done by using the formula given below;

$$\emptyset_{ifgs} = \emptyset_{topo} + \emptyset_{baseline} + \emptyset_{atm} + \emptyset_{def} + \emptyset_{noise} \quad (1.1)$$

where

$\emptyset_{ifgs}$ is interferogram

$\emptyset_{topo}$ is topography phase effect

$\emptyset_{baseline}$ is a baseline error phase

$\emptyset_{atm}$ is an atmospheric phase

$\emptyset_{def}$ is deformation phase

$\emptyset_{noise}$ refers to noise phase contribution.

Instead of noise and baseline error phase, equation (1.1) can be also evaluated as pixel and orbital effect to the interferogram generation. In this way; components of interferometric phase can be defining as (1.2).

$$\Delta\emptyset_{int} = \Delta\emptyset_{orb} + \Delta\emptyset_{topo} + \Delta\emptyset_{atm} + \Delta\emptyset_{pixel} + \Delta\emptyset_{def} \quad (1.2)$$

The phase of an individual interferogram can be divided into five parts:

i. Orbit ($\Delta\emptyset_{orb}$), topography ($\Delta\emptyset_{topo}$) and deformation phase ($\Delta\emptyset_{def}$) are related to the difference distance between the satellite and the ground.

ii. Atmospheric phase $\Delta\emptyset_{atm}$ is related to the difference in the properties of the medium that the radar pulse moves through.

iii. Pixel phase ($\Delta\emptyset_{pixel}$) is related to the change in properties of the pixel on the ground.

A differential interferogram is one in which the effects of orbital baselines and topography have been removed. It is called as DInSAR.

Other components of SAR applications is co-registration that aims to find an optimal transformation model which requires pixel-to-pixel match between common features in SAR image pairs (Li and James, 2008). The precise co-registration rises the coherence of the interferogram, improves the value of the phase unwrapping process and therefore leads to a more accurate phase in the final interferogram (Marinkovic and Ramon, 2004). In this level, a main question comes up "How does InSAR achieve the monitoring

of ground displacement?" The sensitivity of many studies indicate that the accuracy InSAR is~ 0.75 mm in vertical (N-S) and ~ 0.5 mm in horizontal (E-W) direction by using a series of 10-30 images. The difference between the accuracy of N-S and E-W directions depend on many factors like noise in N-S (Samieie-Esfahany et al., 2009). This result has been obtained that in case of a number of high resolution images applied to arid (low vegetation) and structural areas such as buildings, bridges, pipelines, etc., the outcomes are more accurate.

Microwave radiation is emitted as short signals with the help of antennas on the satellite platform. The signals have a specific wavelength, amplitude and polarization. In the properties of signals sent to the target on the earth. There are some changes in the transmission and recovery process throughout the atmosphere. These signals are reversed by the same antenna and recorded in phase, polarization and amplitude. Finally, the image production process, which varies depending on the satellite sensor and which covers the target area, is realized (eg IS2-mode image size for ASAR data of Envisat 100 km x 100 km, ALOS PALSAR data (FBS mode) 70 km x 70 km (including a frame).

Perpendicular sensor-target direction to satellite orbit; the direction of the radar (Line of Sight -LOS) or the oblique length. The coordinates of a radar image consist of the target-sensor distance and the position component shown along the trajectory of the sensor. The second is called azimuth. The geometric description of the SAR system is shown in figure 2 with the geometric elements.

The coordinate system of a SAR image is different from the location coordinate (or geographic) coordinate system. x and y axes are considered as latitude and longitude in geographic system, but in SAR system it is considered as azimuth and slant range (Figure 3).

2.1. Ascending and Descending Pass

Satellite platforms produce images according to two different modes, increasing and decreasing. The geometry of the ascending mode occurs at the South-North transition of the satellite and the target is observed from the west, while in the descending mode the target is observed from the east during the North-South transition.

The basis of the observation of the SAR satellites is that they display the surface as inclined instead of

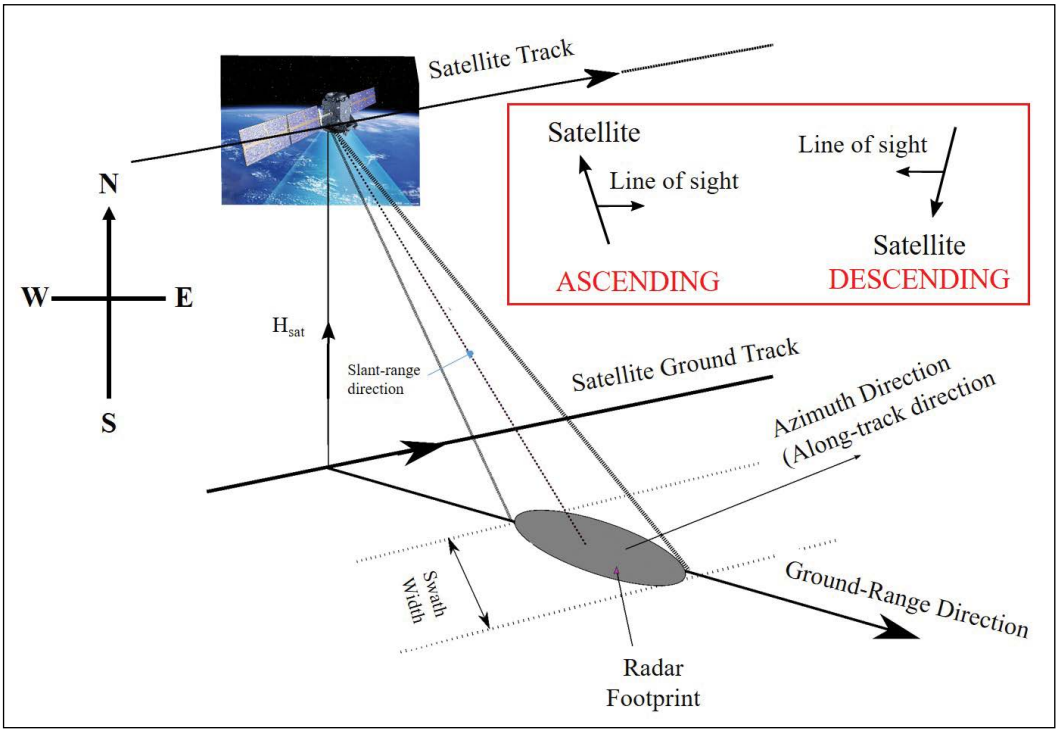

Figure 2- Geometric description of the SAR system.

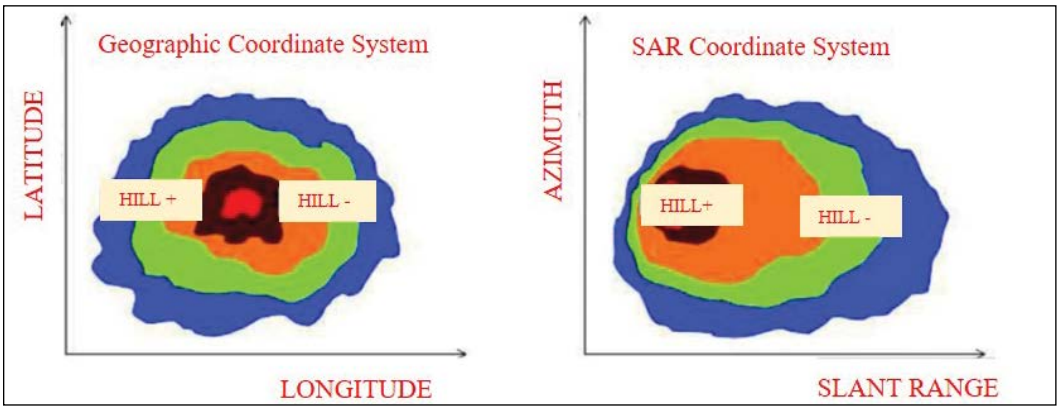

Figure 3- Comparison of Geographic Coordinates with SAR coordinates (by changing from Hooper, 2006).

vertical. When the ground moves west, the ground motion is close to the satellite if the satellite is observing the orbit that is increasing in the north. On the contrary, if the satellite is observing in the descending mode towards the south, ground motion is far from the satellite (Figure 4).

The numbers written under the color chart in figure 4. shows distance between the ground and the satellite from line-of-sight (LOS) of the satellite. Negative values indicate that the distance between the satellite and the ground is reduced. In this study, it has been used both data from ascending and descending orbits to recognize certain displacement and compare the results for clear understanding the fault track between each interferograms.

2.2. DInSAR Processing Steps

All InSAR processing steps except phase unwrapping stage, have been calculated with using SNAP (Sentinel Application Platform) software which is free for remote sensing software users created by ESA (European Space Agency). Processing steps were started with co-registrating master and slave images, interferogram formation, topographic phase removing, phase filtering and phase unwrapping which is the last and one of the most critical step of InSAR processing made using by SNAPHU (Statistical-Cost, Network-Flow Algorithm for Phase Unwrapping). 'Unwrapping' is the process of converting the cyclical (modulo 2π) phase signal of an interferogram into a continuous phase signal. It is usually preferable to use unwrapped phase for deformation or topography estimation. After all steps completed successfully, geocoding step (conversion of phase values from Line

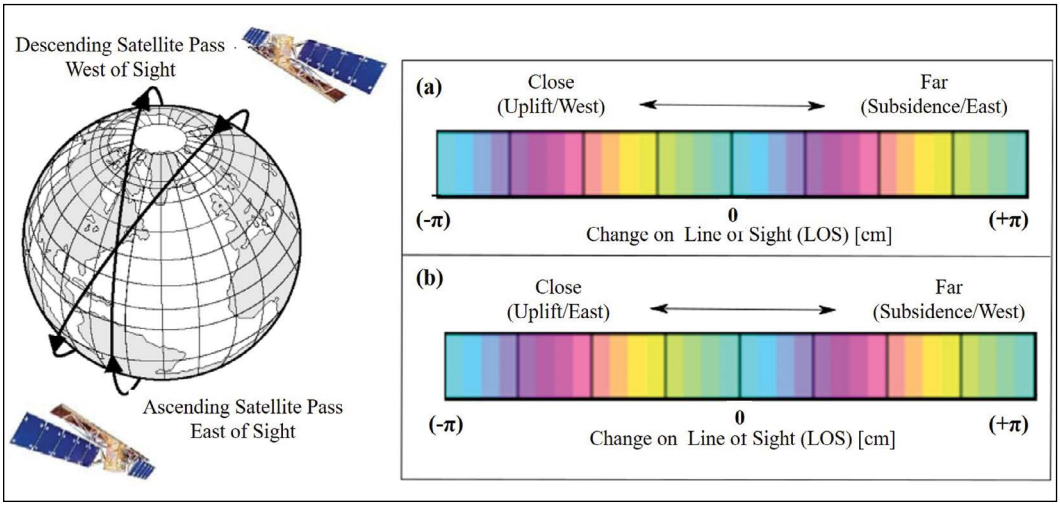

Figure 4- Schematic representation of the polar orbital satellites with an east and west view perspective, (Left panel). a) observations from ascending and b) descending orbits (right panel) (by from Çomut, 2016).

of Sight to Ellipsoidal Height) done for geo-location.

Briefly; a typical DInSAR processing chain in practice will have multiple steps, usually in this order:

1) Matching (co-registering) the SLCs
2) Forming the interferogram by differencing phases
3) Removing the effects of orbit position and Earth curvature
4) Registering the interferogram to a DEM; removing the effects of topography
5) Filtering and unwrapping

The detailed explanation of DInSAR processing flow chart is shown in figure 5.

3. Study Area

The Zagros fold-and-thrust belt is the world's most seismically active mountain ranges, and is influential in our understanding of continental collisions. It is almost 1500 km in length and ~300 km wide around the south-western Iran and a major structural element of the Alpine–Himalayan belt (Nissen et al., 2007, 2010 and 2011). This belt extends towards northwest up to Taurides in Turkey. Because of the continuation in mountainious topography, the suture zone represents the geological units related to collision of Eurasian and Arabian plates, it is called as Bitlis-Zagros suture zone in literature. Zagros fold belt is an important structure due to the accumulation of hydrocarbons that provides 2/3 oil and 1/3 gas-resources of the world. The accumulation is directly related to the stratigraphy and structural evolution of the belt (Alavi,

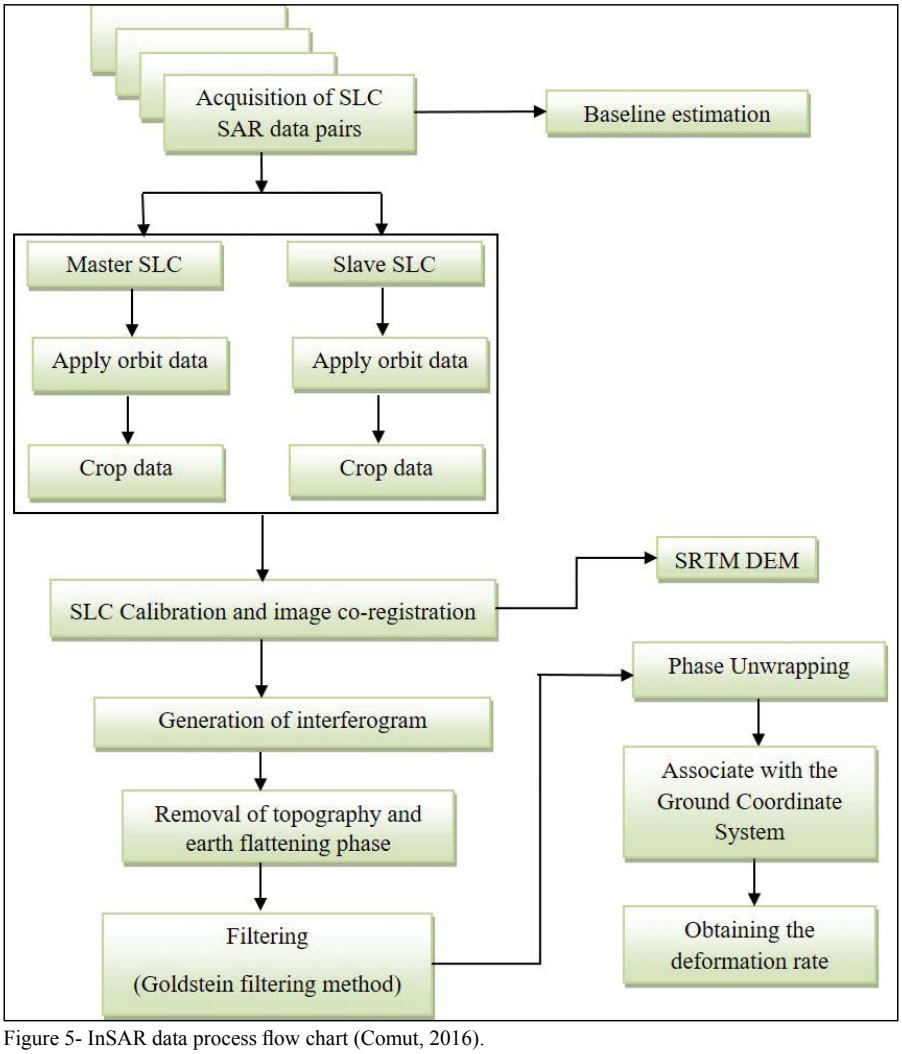

Figure 5- InSAR data process flow chart (Comut, 2016).

2007). This situation results a number of studies based on stratigraphy and geophysical exploration of SW verging folds and NW-SE trending thrust-reverse fault system (Colman-Sadd, 1978; McQuarrie, 2004; Dehbozorgi et al., 2010) (Figure 6). Furthermore, there are several studies related to the earthquakes in the area. Because of the very rare (Walker et al., 2005) and usually absent indications of coseismic ruptures at the surface, these earlier studies concluded that the larger earthquakes in the Zagros involve faulting mostly within the basement. However, more recent geodetic studies, which use radar interferometry (InSAR) to determine the depth extents of coseismic faulting, have revealed that moderate-sized earthquakes (up to Mw ~6) also occur within the sedimentary cover, rupturing between depths of ~4 and ~9 km (Nissen et al., 2007, 2010; Roustaei et al., 2010).

Zagros fault system which is the boundary between Arabian plate in the SW and Eurasian plate in the NE is a seismically active area experiencing a number of huge earthquakes. The events are the main reason for the deformation of the area by means of convergent plate motions. According to the fault mechanism solutions of different observartory centers (Figure 7), the strike of source fault is approximately NNW-SSE and dipping towards NE. The configuration of the hangingwall and footwall blocks indicate that NE block (hanging block) of the fault is uplifted. The key point what is the amount of uplift or vertical displacement near epicentral area. In November 12th 2017, a devastating earthquake with M=7.3 happened around Sarpol-e Zahab town. The epicenter location is determined near the border of Iraq-Iran according to USGS (34.905°N 45.956°E, 22.0 km depth).

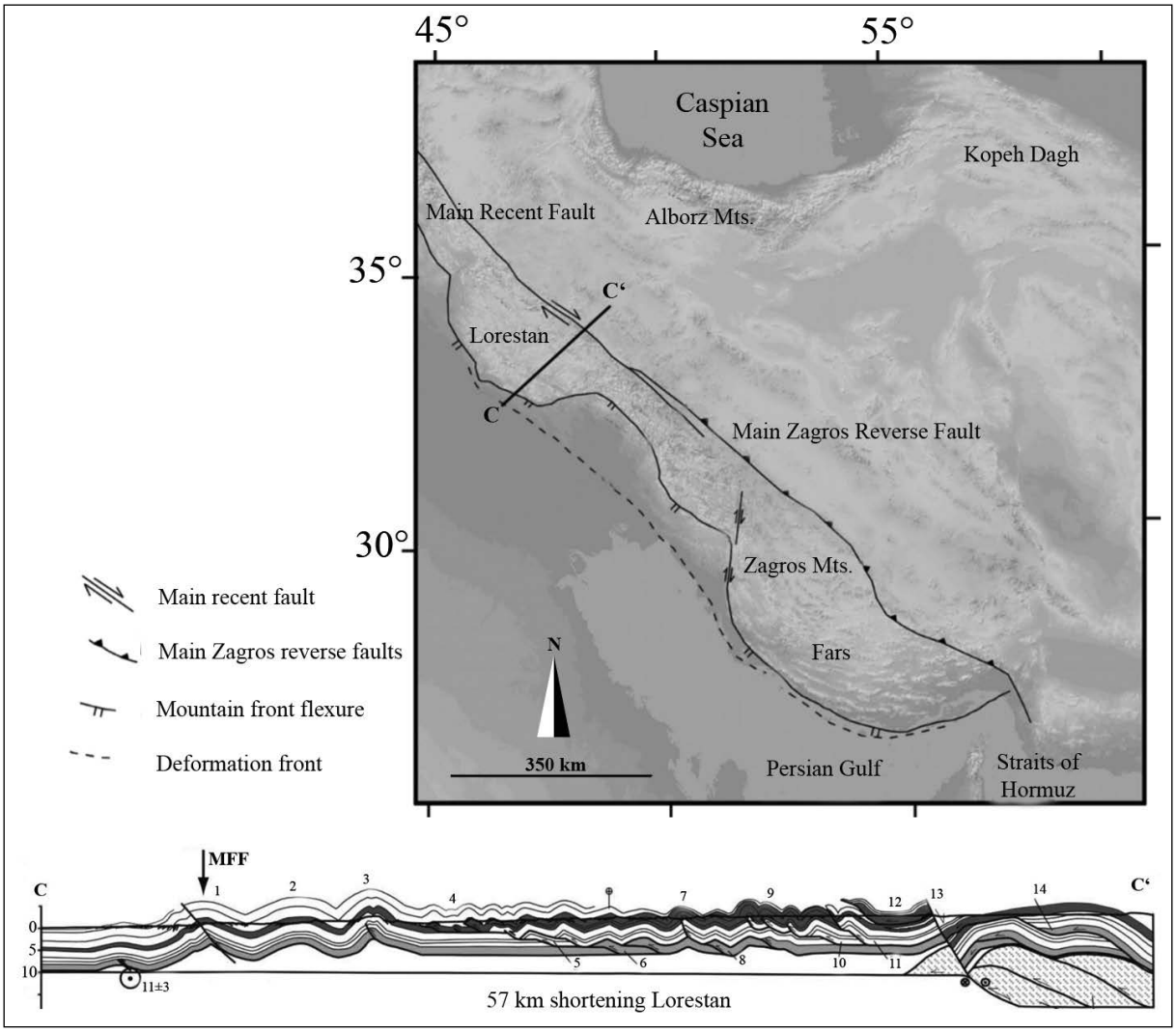

Figure 6- Location of the Zagros fault system and cross-section of epicentral area C-C' (McQuarrie, 2004).

Eigth different observatory centers figured out focal mechanism solutions of the earthquake and they are mostly the same attitude thrust faulting with minor strike slip component (Figure 7). The convergent plate boundary between Arabian and Eurasian creates such strong seismic activities and a significant infrastructure damages had caused, over 530 people were killed and 8000 were injured.

Even though there are a number of geological studies in literature related to the area that is a huge laboratory for the plate motions, we focused on the surface deformation because of the earthquake by means of SAR analyses. A series of SAR images have been obtained from Sentinel-1. The intensity of the SAR image directly corresponds to terrain slope and surface roughness, the AOI (Area of Interest) have rough topography with rugged terrain, mountains and rivers (Figure 8). Selecting ascending or descending paths is very important step to determine the deformation from different angles. If the selection has not been done properly, InSAR does not give the best results.

4. Data

Four scenes of Sentinel-1 C-band were used for InSAR processing that areas represented in table 1. All scenes are vertical-transmit and vertical-receive

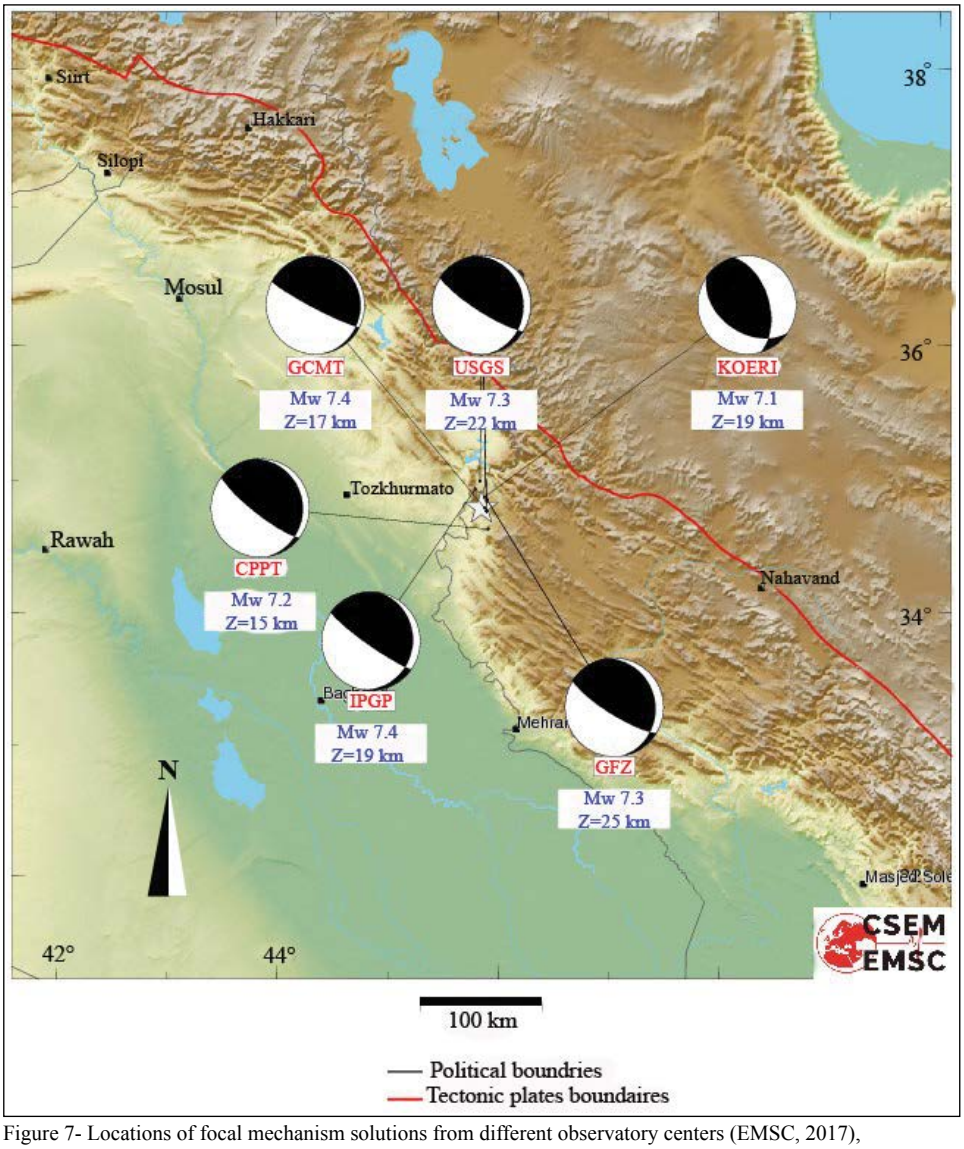

Figure 7- Locations of focal mechanism solutions from different observatory centers (EMSC, 2017), https://earthquake.usgs.gov/earthquakes/eventpage/us2000bmcg#region-info.

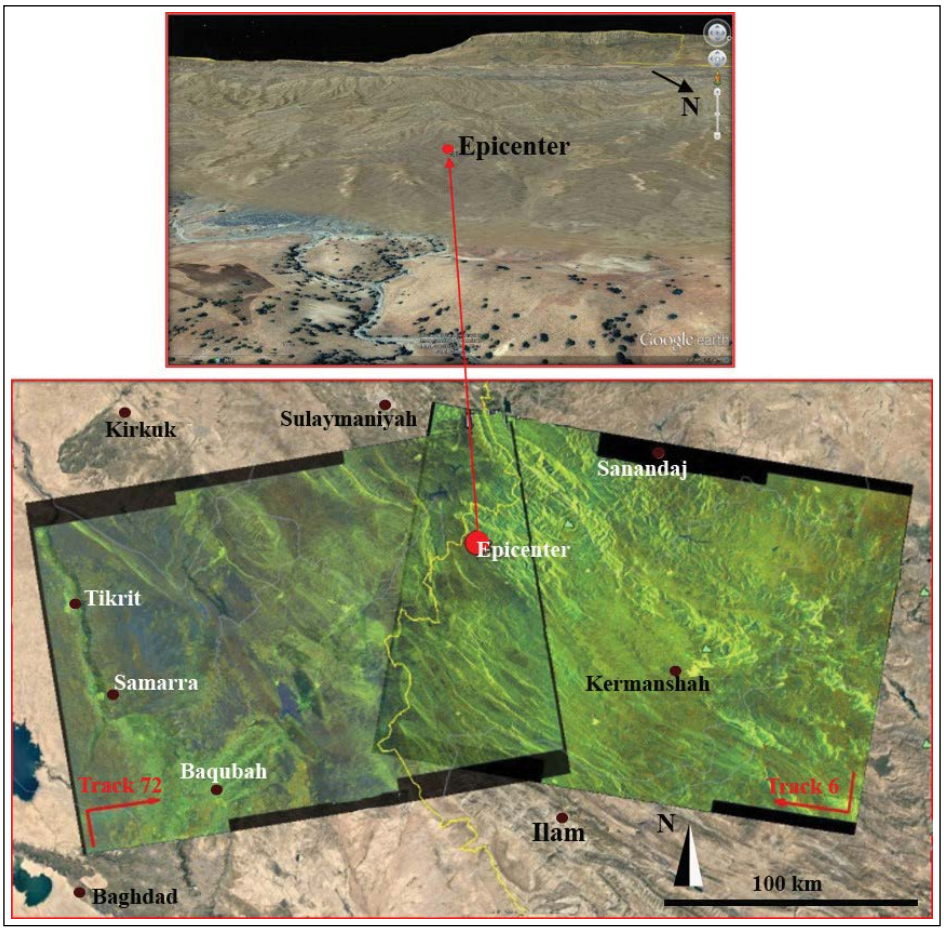

Figure 8- AOI Relief map, Iran and the frames of the ascending (left) and descending (right) configuration of Sentinel-1 image used for the study (base maps are from Google earth).

Table 1- Characteristics of Sentinel-1 InSAR pairs for the 72 and 6 Tracks (B_{tem}: temporal baseline, B_{per}: perpendicular baseline).

Track	**72 VV**		**6 VV**	
Pass	ASCENDING		DESCENDING	
Date	11/11/2017	11/17/2017	11/07/2017	11/19/2017
B_{per} (m)	62.22		14.44	
B_{temp} (m)	6		12	
Height Ambiguity (m)	252.47		1087.6	
Orbit	19219	8323	19328	19153
SENTINEL	1A	1B	1A	1A

(VV) polarized. The SAR images cover southern Halabja (30 km). The incidence angles of Sentinel-1 are approximately 20° to 46°, and have wavelength of 5.546 cm.

5. SAR Interferometric Analyses

To infer co-seismic land uplift and subsidence, we had used Sentinel-1 data, and Differential InSAR method (DInSAR). This technique allows investigating where and how the crust deform near of the epicenter. DInSAR processing is monitoring surface movement by computing a differential interferogram of the same SAR data from two repeat pass acquisitions. Figure 9 presents the differential phase interferograms from the ascending and descending orbits of the AOI.

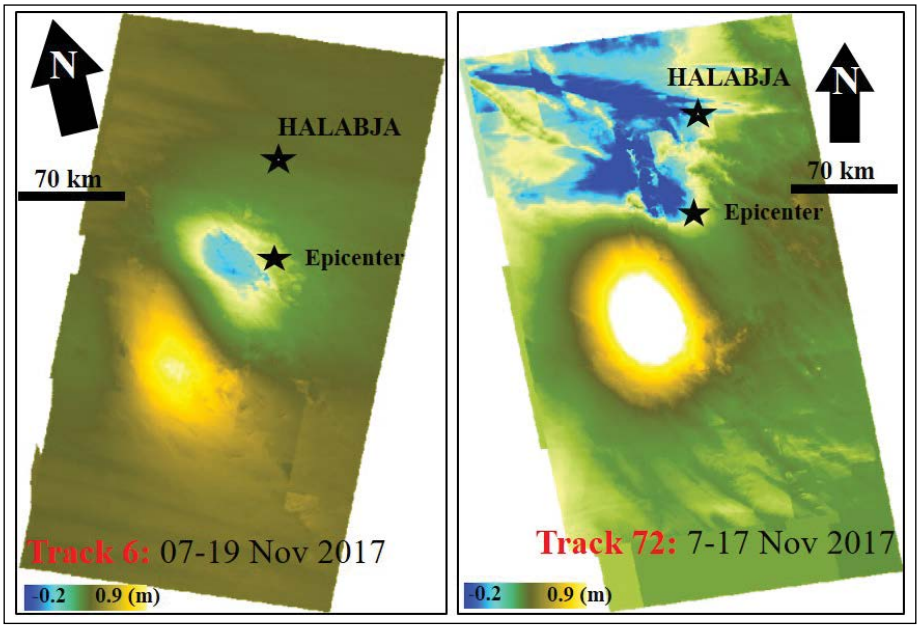

Figure 10- Deformation map along the LOS. After phase unwrapping and phase to displacement conversion.

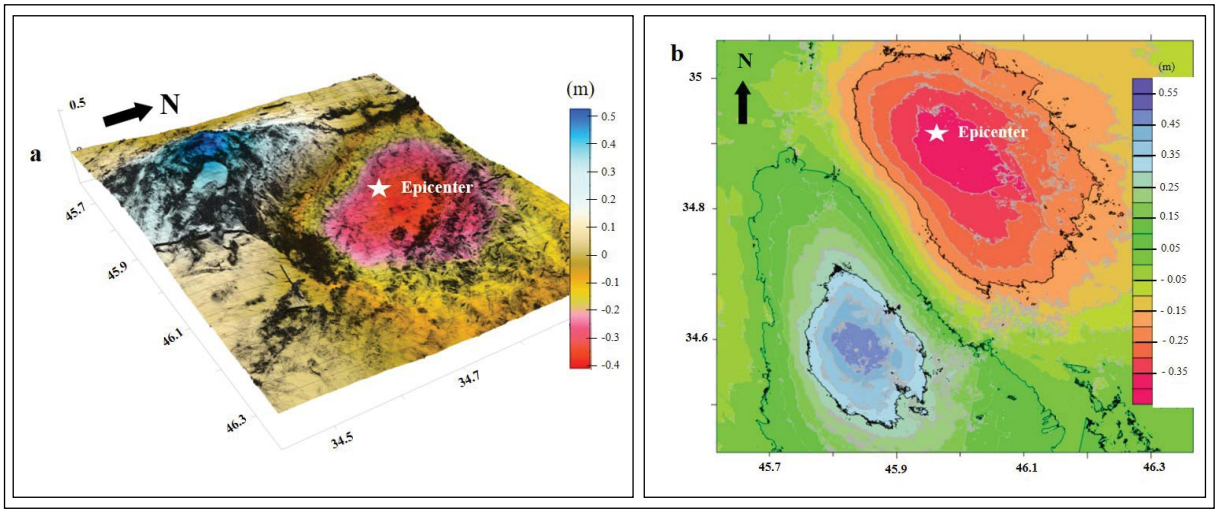

Figure 11- a) 3D view deformation map of the track6 (07-19 November 2017) and b) contour map along LOS displacement.

are reported in Appendix A, including noise and atmospheric phase effects for the analysed cases.

6. Damages in the Infrastructures

The buildings in the cities and villages are suspected to be submitted for deformation. In both cases subsidence or uplift, the infrastructures may experience heavy damages. Figure 12 represents 3D view deformation map of the track 6 (07-19 November 2017). The black line is approximate strike of fault at the surface and ~ N35°W striking direction inferred from InSAR. The greatest damage is considered to be on the fault line shown in figure 1 and in its vicinity.

During field observation by AFAD committee it is seen that many infrastructures get damaged. Due to seismic reports from Zare et. al., (2017); "8.000 injured, 70.000 displaced, and over 12.000 buildings have been damaged". Associated with this earthquake

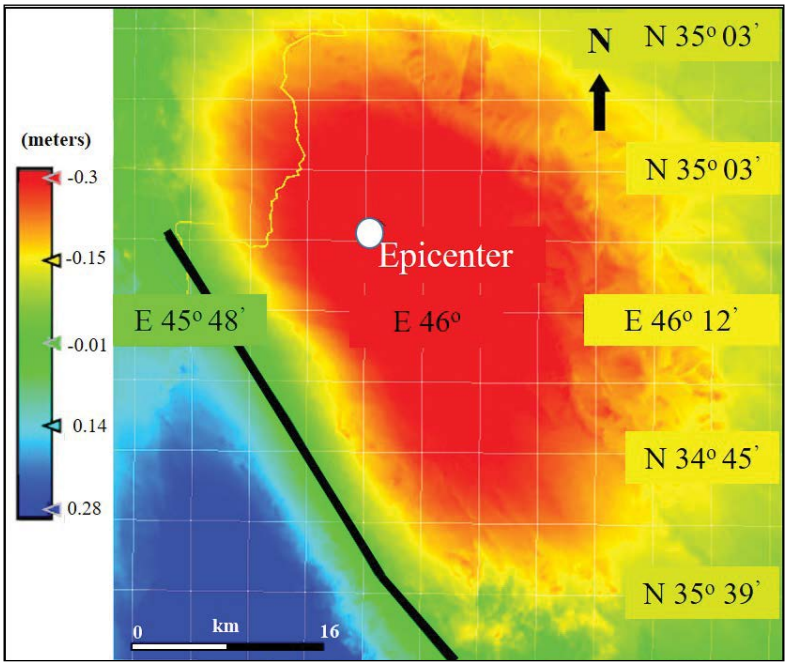

Figure 12- 3D view deformation map of the track 6 (07-19 November 2017), the black line is suspected fault location and direction inferred from InSAR and the location of villages.

and its aftershocks, approximately 5,000 buildings in the disaster impact area were heavily damaged beyond repair (Figure 13).

7. Conclusions

Zagros Mountains is the result of mountain range between two plates (Şengör and Kidd, 1979; Dewey et al., 1986; Dilek et al., 2009; Ghalamghash et al., 2016; Fahim Guilany et al., 2019). The plates' motions create high earthquake activitiy and remarkable surface topography. After Iran earthquake, we would like to test the ability of DInSAR method to detect the surface motion in vertical scale. The present paper has two main objectives; one of them is to reveal the surface deformation caused by Mw 7.3 2017 Iran Earthquake in (12 November 2017), and second is to determine the strike of fault line at the surface by using InSAR method without visiting the study area. Before testing the results without ground truth data,

Figure 13- Photos from study area, a) photo from one damaged house, b) AFAD President's investigation over damaged dam (taken by AFAD) and c) general scene from destroyed houses (Google search).

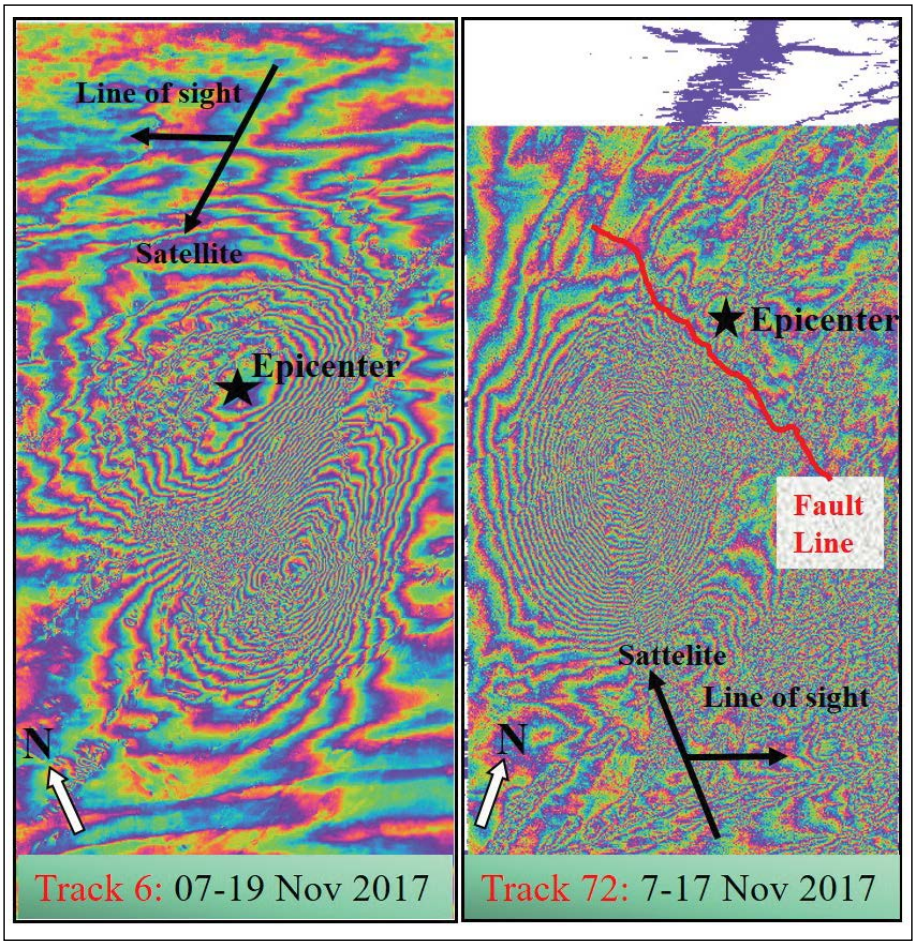

Figure 9- Interferograms from Sentinel-1 InSAR pairs, each fringe is colored by the cycle of $-\pi$ to π.

The interferograms generated confirmed the existence of deformation surrounding the epicenter. The amount of displacements and its directions calculated after the phase unwrapping reveals a huge deformation area reach 90 cm and -41 cm, and it extend to 80 km from the location of epicenter. Yellow spot indicates the uplifted and the blue spot represent subsided areas in figure 10.

The maximum and minimum displacement values from the ascending and descending orbit of the scene are calculated as:

Track 06 = 07-19 November 2017 Min: -0.411, Max: 0.526m

Track 72 = 11-17 November 2017 Min: -0.191, Max: 0.898m

The track 72 in figure 10; due to 'blue spots' indicates some differences from the track 6. At first look; ever if the "blue colour change" demonstrates displacement in track 72, when the area with blue interpret with topography (Figure 8) and the wrapped interferogram phase (Figure 9), it is clear that this colour changes result is only because of unwrapping errors or no Data representation. Therefore, unwrapping error and less data; low coherent zone represents the 'blue spot' area. After re-masking the interferogram, the unwrapping result cannot be fully improved to get better result without scattered blue zone. More examples of InSAR measurements for aftershocks of the earthquake are reported in Appendix A to show similar results.

Figure 11(a) represents surface deformation of the AOI on the digital elevation model and (b) contour map of the same area along the LOS. It can be said from the deformation shape that two blocks of the fault moved significantly in vertical direction. More examples of fitted monitored displacements for the study area affected by the earthquake of aftershocks

the amount of displacement could be obtained by processing two different acqusition mode which are ascending (from S to N) and descending (from N to S). To determine the surface deformation, one of the phases could be used in case of a landslide but in an earthquake, descending and ascending track modes of the satellite should be used. The difference between descending and ascending interferograms is that SAR interferogram shows the displacement only in the direction where the ground moves close to or away from the satellite. As a result, in spite of detecting the same deformation, an interferogram from ascending orbits different to one from descending orbits. As such, it is difficult to determine the direction of displacement using a single SAR interferogram, but determination of the direction can be made by comparison of InSAR data with GPS measurement data, or by combining the several data from different directions (i.e. ascending and descending).

In our study, two modes were used to find out the uplift and subsidence in both blocks of the fault. As conclusions, the potential of SAR image was investigated for assessment of vertical displacement caused by the earthquake in the field of Halabja. The summaries are given below:

1. The deformation is observed straight up and surrounding the Epicenter.
2. Approximate fault strike is detected in the direction of ~ N35°W.
3. The analysis of the deformation has revealed that the ground reach more than – 40 cm subsidence in the footwall (in the SW of fault line) and + 90 cm uplift in the hangingwall block (in the NE of fault line).
4. Fault detection is possible to track with DInSAR. The estimation of its horizontal displacement is a challenge to be inferred.

Acknowledgements

Authors are grateful to have provided freely the Sentinel-1A/B data by European Space Agency (ESA) through Copernicus Programme. Sentinel-1 precise orbit ephemerides were acquired from ESA Sentinel-1 Quality Control group. Authors also acknowledge the use of Google Earth to display the result.

References

Alavi, M.A. 2007. Structures of the Zagros Fold-Thrust Belt in Iran. American Journal of Science 307, 1064-1095.

Ambraseys, N.N., Melville, C.P. 1982. A History of Persian Earthquakes, Cambridge University Press, Cambridge.

Colman-Sadd, S.P. 1978. Fold development in Zagros simply folded belt, Southwest Iran. Am Assoc Petrol Geol Bull 62, 984–1003.

Çomut, F.C. 2016. Farklı yeryüzü özelliklerinde ileri InSAR teknikleri kullanılarak yüzey deformasyonlarının belirlenmesi (Doctoral dissertation, Selçuk Üniversitesi Fen Bilimleri Enstitüsü).

Dehbozorgi, M., Pourkermani, M., Arian, M., Matkan, A.A., Motamedi, H. Hosseiniasl, A. 2010. Quantitative analysis of relative tectonic activity in the Sarvestan area, central Zagros , Iran. Geomorphology 121, 329-341.

Dewey, J. F., Hempton, M.R, Kidd, W.S.F., Şaroğlu, F., Şengör, A.M.C. 1986. Shortening of continental lithosphere: The neotectonics of eastern Anatolia-a young collision zone, in Collosion Tectonics (Coward, M.P., and Ries, A.C., edts.), Geological Society Special Publications 19, 3-36.

Dilek, Y., Imamverdiyev, N., Atunkaynak, S. 2009. Geochemistry and tectonics of Cenozoic volcanism in the Lesser Caucasus (Azerbaijan) and the peri-Arabian region: collision-induced mantle dynamics and its magmatic fingerprint. International Geology Review 1-42, DOI:10.1080/00206810933604422.

Emami, H., Vergés, J., Nalpas, T., Gillespie, P., Sharp, I., Karpuz, R., Blanc, E. P., Goodarzi, M.G.H. 2010. Structure of the Mountain Front Flexure along the Anaran anticline in the Pusht-e Kuh Arc (NW Zagros, Iran): insights from sand box models. Geological Society, London, Special Publications 330, 155-178.

EMSC, 2017. https://www.emsc-csem.org/Earthquake/260/M7-3-Iran-Iraq-Border-Region-on-November-12th-2017-at-18-18-UTC

Fahim Guilany, R., Darvishzadeh, A., Sheikhzakariaee, S.J., Vosoughi Abedini, M. 2019. Geochemical characteristics of Sabalan volcanic rocks in Northwestern Iran. Bulletin of the Mineral Research and Exploration 158, 217-233.

Falcon, N. L. 1974. Southern Iran: Zagros Mountains. In: SPENCER, A. M. (ed.) Mesozoic–Cenozoic Orogenic Belts. Data for Orogenic Studies. Geological Society, London, Special Publications 4, 199–211.

Ferretti, A., Bianchi, M., Prati, C., Rocca, F. 2005. Higher-Order Permanent Scatterers Analysis. – EURASIP Journal on Applied Signal Processing 20, 3231–3242.

Ghalamghash, J., Mousavi, S.Z., Hassanzadeh, J., Schmitt, A.K. 2016. Geology, zircon geochronology, and petrogenesis of Sabalan volcano (Northwestern Iran). Journal of Volcanology and Geothermal Research 327, 192-207. Doi: 10.1016/j.

Goudarzi, M.A. 2010. Detection and measurement of land deformations caused by seismic events using InSAR, sub-pixel correlation and inversion techniques. University of Twente Faculty of Geo-Information and Earth Observation (ITC). jvolgeores.2016.05.001

Hanssen, R. F. 2001. Radar interferometry: Data interpretation and error analysis. Dordrecht: Kluwer Academic Publishers 328 pp. ISBN 0-7923-6945-9.

Hooper, A. J. 2006. Persistent scatter radar interferometry for crustal deformation studies and modeling of volcanic deformation, AAI3219289; ISBN: 9780542706905, Stanford University, 124 p.

https://earthquake.usgs.gov/earthquakes/eventpage/us2000bmcg#region-info

https://sentinels.copernicus.eu/web/sentinel/technical-guides/sentinel-1-sar/sar-instrument

Intrieri, E., Gigli, G., Casagli, N., Nadim, F. 2013. Brief communication Landslide Early Warning System: Toolbox and general concepts, Natural Hazards and Earth System Science 13(1), 85–90, doi:10.5194/nhess-13-85-90.

Kim, J. W. 2013. Applications of Synthetic Aperture Radar (SAR)/SAR Interferometry (InSAR) for Monitoring of Wetland Water Level and Land Subsidence. The Ohio State University.

Li, Z., James, B. 2008. Image coregistration in SAR interferometry. The International Archives of the Photogrammetry. Remote Sensing and Spatial Information Sciences 37, 433-438.

Marinkovic, P., Ramon, H., 2004. Advanced InSARcoregistration using point clusters. Geoscience and Remote Sensing Symposium, 2004. IGARSS'04. Proceedings. 2004 IEEE International. Vol. 1. IEEE

McQuarrie, N. 2004. Crustal scale geometry of the Zagros fold-thrust belt, Iran. J Struct Geol 26, 519–535.

Netzband, M,, William, L. S., Charles, R. 2007. Applied remote sensing for urban planning, governance and sustainability. Springer Science & Business Media.

Nissen, E., Ghorashi, M., Jackson, J., Parsons, P., Talebian, M. 2007. The 2005 Qeshm Island earthquake (Iran) – a link between buried reverse faulting and surface folding in the Zagros Simply Folded Belt? Geophys J Int 171, 326–338.

Nissen, E., Yamini-Fard, F., Tatar, M., Gholamzadeh, A., Bergman, E., Elliott, J.R., Jackson, J.A., Parsons, B. 2010. The vertical separation of mainshock rupture and microseismicity at Qeshm island in the Zagros Simply Folded Belt, Iran. Earth Planet Sci Lett 296, 181–194.

Nissen, E., Tatar, M., Jackson, J.A., Allen, B. 2011. Geodynamics and tectonics New views on earthquake faulting in the Zagros fold-and-thrust belt of Iran. Geophys J Int doi: 10.1111/j.1365-246X.2011.05119.x.

Pritchard, M, E. 2006. InSAR, a tool for measuring Earth's surface deformation. Physics Today 59, 7, 68.

Samieie-Esfahany, S., Hanssen, R., Karin van Thienen-Visser, Annemarie, M. 2009. On the Effect of Horizontal Deformation on InSAR Subsidence Estimates. In Proceedings of the Fringe 2009 Workshop, ESA SP, 677.

Şengör, A.M.C., Kidd, W.S.F. 1979. Post-collisional tectonics of the TurkishIranian. Plateau and a comparison with Tibet, Tectonophysics 55, 361-376.

Thiebes, B. 2012. Integrative Early Warning. Landslide Analysis and Early Warning Systems. Springer Berlin Heidelberg, 215-219.

Walker, R.T., Andalibi, M.J., Gheitanchi, M.R., Jackson, J.A., Karegar, S., Priestley, K. 2005. Seismological and field observations from the 1990 November 6 Furg (Hormozgan) earthquake: a rare case of surface rupture in the Zagros mountains of Iran. Geophys J Int 163, 567–579.

Zare, M., Kamranzad, F., Parcharidis, I., Tsironi, V. 2017. Preliminary report of Mw7. 3 Sarpol-e Zahab, Iran earthquake on November 12, 2017. EMSC Report 1-10.

Appendix A: Estimation of Co-Seismic Land Deformation Due to Mw 5.5, 11 January 2018 Iran Earthquake by Mean of DInSAR Technique

This section reports the larger-area interferograms of different date combinations. SAR image dates were selected to display the effects of two earthquakes, particularly on 11 January 2018, of 5.5 Mw and 5.4 Mw (Mw 5.5 – 18 km E of Mandali, Iraq 2018-01-11 06:59:31 UTC 33.764°N 45.749°E10.0 km, Mw 5.4 - 14km E of Mandali, Iraq 2018-01-11 08:00:40 UTC 33.774°N 45.710°E10.0 km). From each interferogram it can be seen various errors, due to weather conditions in some of the dates. But some of them also indigates significant information about displacement along the fault zone.

Table A1- Characteristics of Sentinel-1 InSAR pairs for the 72 and 6 Tracks. https://sentinels.copernicus.eu/web/sentinel/technical-guides/sentinel-1-sar/sar-instrument

Track	**6 VV**	
Pass	DESCENDING	
Date	**1/6/2018 2:54**	**1/18/2018 2:54**
Bper	-64.88	
Btem	12	
Height Ambg m	242.16	
Orbit	20028	20203
SENTINEL	1A	1A
Track	**6 VV**	
Pass	DESCENDING	
Date	**12/31/2017 2:53**	**1/18/2018 2:54**
Bper	10.3	
Btem	18	
Height Ambg m	-1515.86	
Orbit	8957	20203
SENTINEL	1B	1A
Track	**6 VV**	
Pass	DESCENDING	
Date	**1/6/2018 2:54**	**1/12/2018 2:53**
Bper	21.25	
Btem	6	
Height Ambg m	734.99	
Orbit	20028	9132
SENTINEL	1A	1B
Track	**6 VV**	
Pass	DESCENDING	
Date	**12/31/2017 2:53**	**1/12/2018 2:53**
Bper	-34.94	
Btem	12	
Height Ambg m	446.88	
Orbit	8957	9132
SENTINEL	1B	1B
Track	**72 VV**	
Pass	ASCENDING	
Date	**1/4/2018 14:59**	**1/16/2018 14:59**
Bper	62.22	
Btem	6	
Height Ambg m	252.47	
Orbit	9023	9198
SENTINEL	1B	1B

($\mathbf{B}_{tem}$: temporal baseline, $\mathbf{B}_{per}$: perpendicular baseline).

06 January 2018 - 18 January 2018 06 VV – DESCENDING

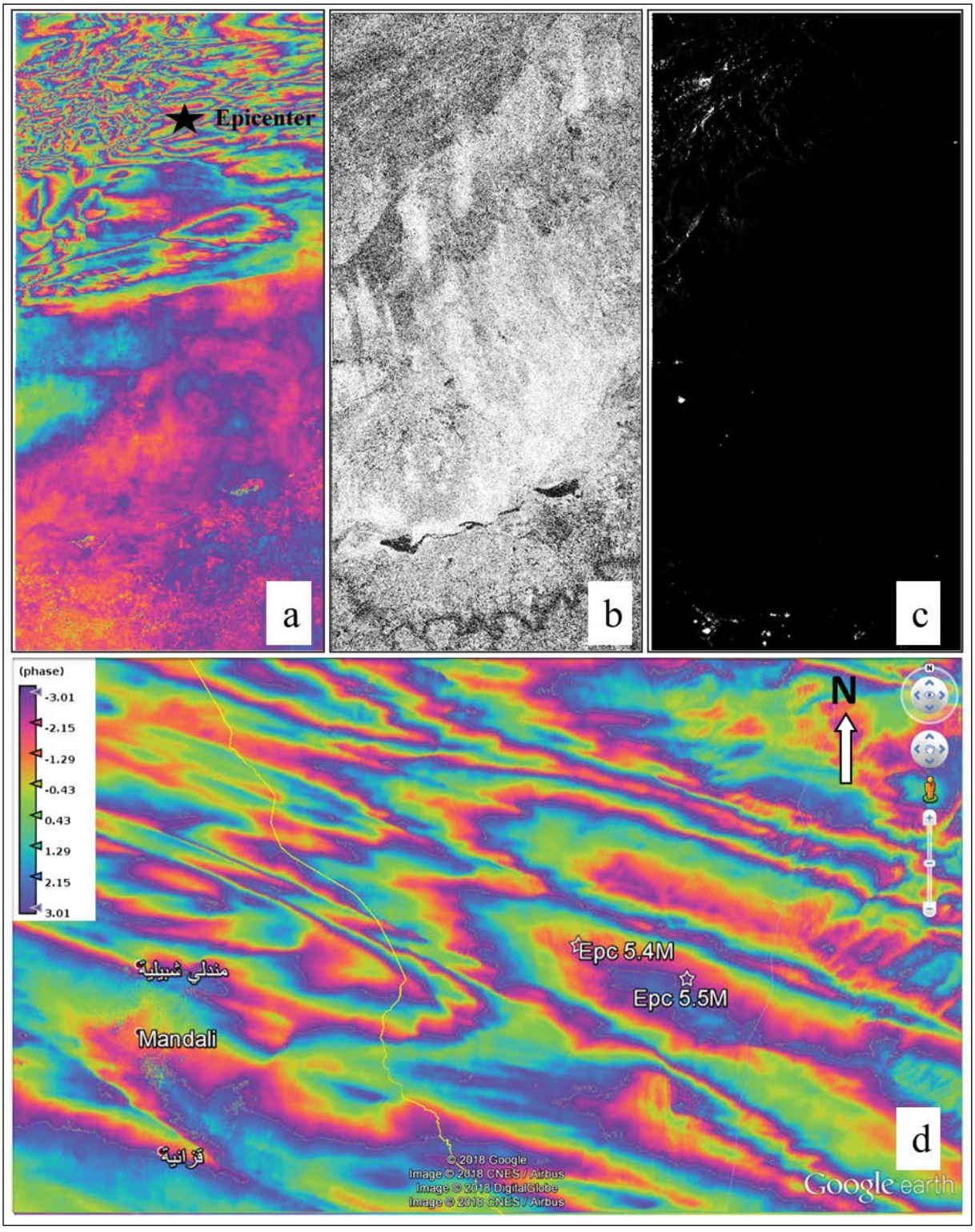

Figure A1- Interferograms from Sentinel-1 InSAR pairs (06 January 2018 - 18 January 2018 06 VV – DESCENDING), a) interferogram, b) intensitiy, c) coherence maps and d) filtered interferogram. There is no information about displacement due to atmospheric errors.

31 December 2017 - 18 January 2018 06 VV – DESCENDING

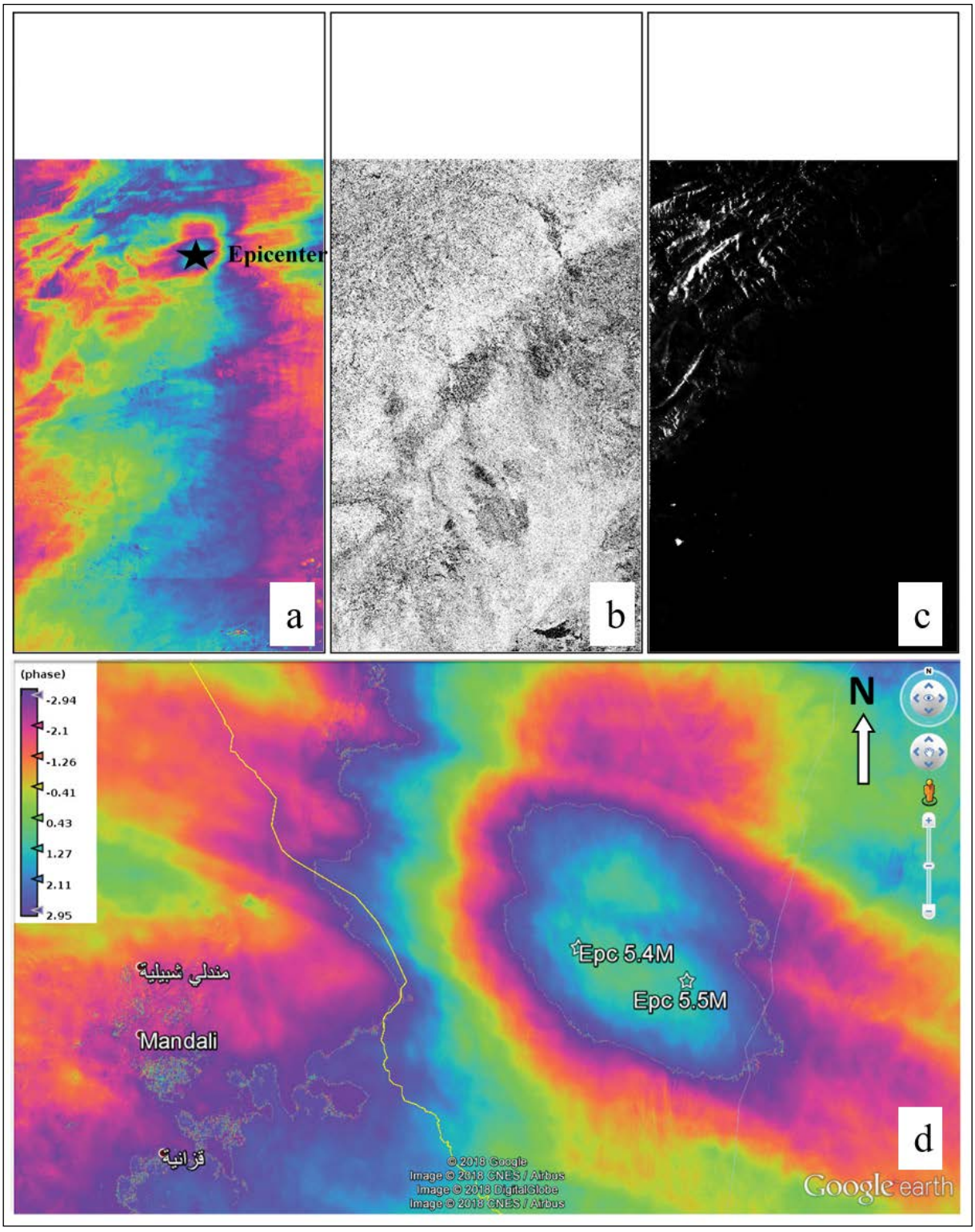

Figure A2- Interferograms from Sentinel-1 InSAR pairs (31 December 2017 - 18 January 2018 06 VV - DESCENDING), a) interferogram, b) intensitiy, c) coherence maps and d) filtered interferogram. Each fringe is colored by the cycle of $-\pi$ to π.

06 January 2018 - 12 January 2018 06 VV – DESCENDING

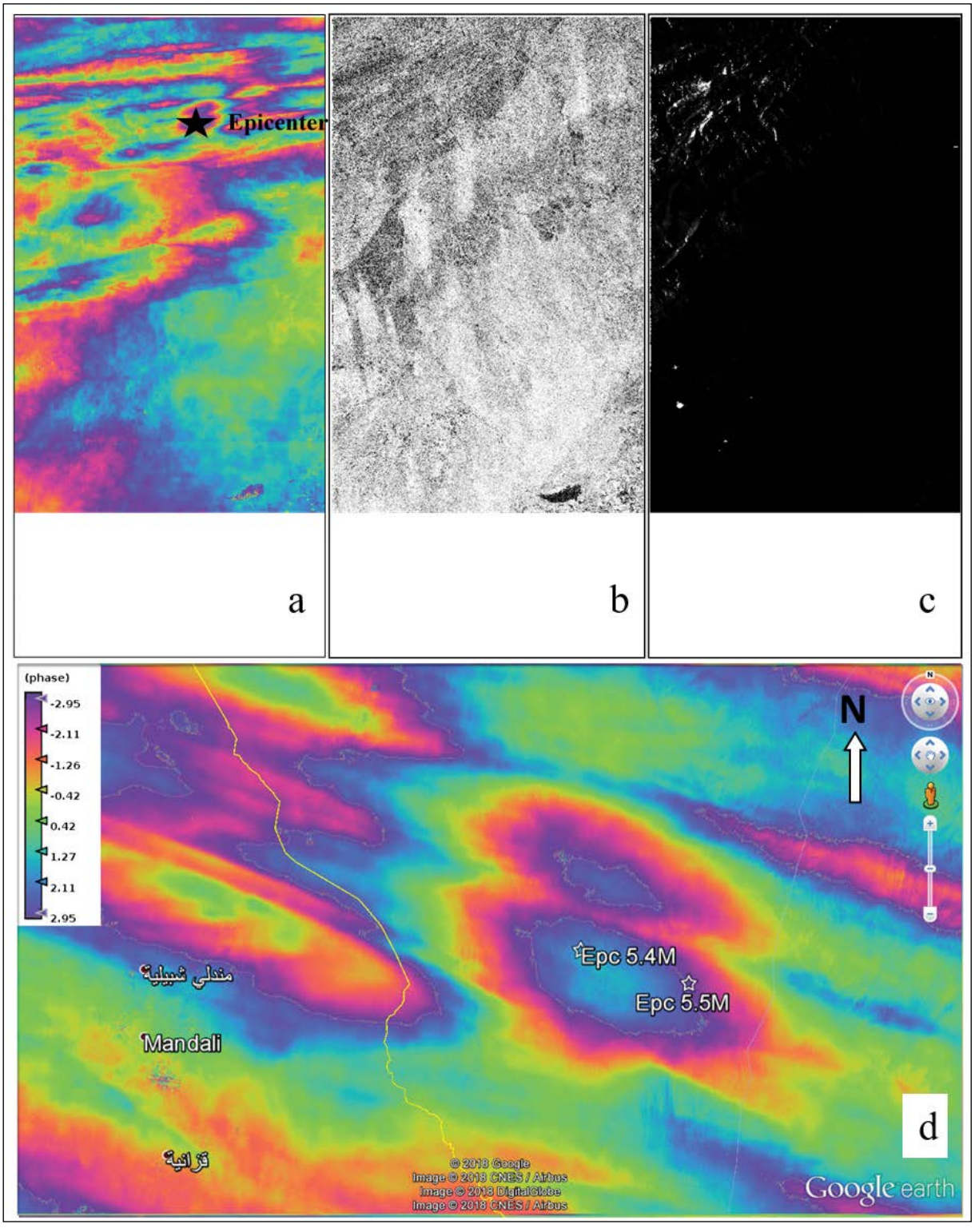

Figure A3- Interferograms from Sentinel-1 InSAR pairs (06 January 2018 - 12 January 2018 06 VV – DESCENDING), a) interferogram, b) intensitiy, c) coherence maps and d) filtered interferogram. Each fringe is colored by the cycle of $-\pi$ to π.

31 December 2017 - 12 January 2018 06 VV – DESCENDING

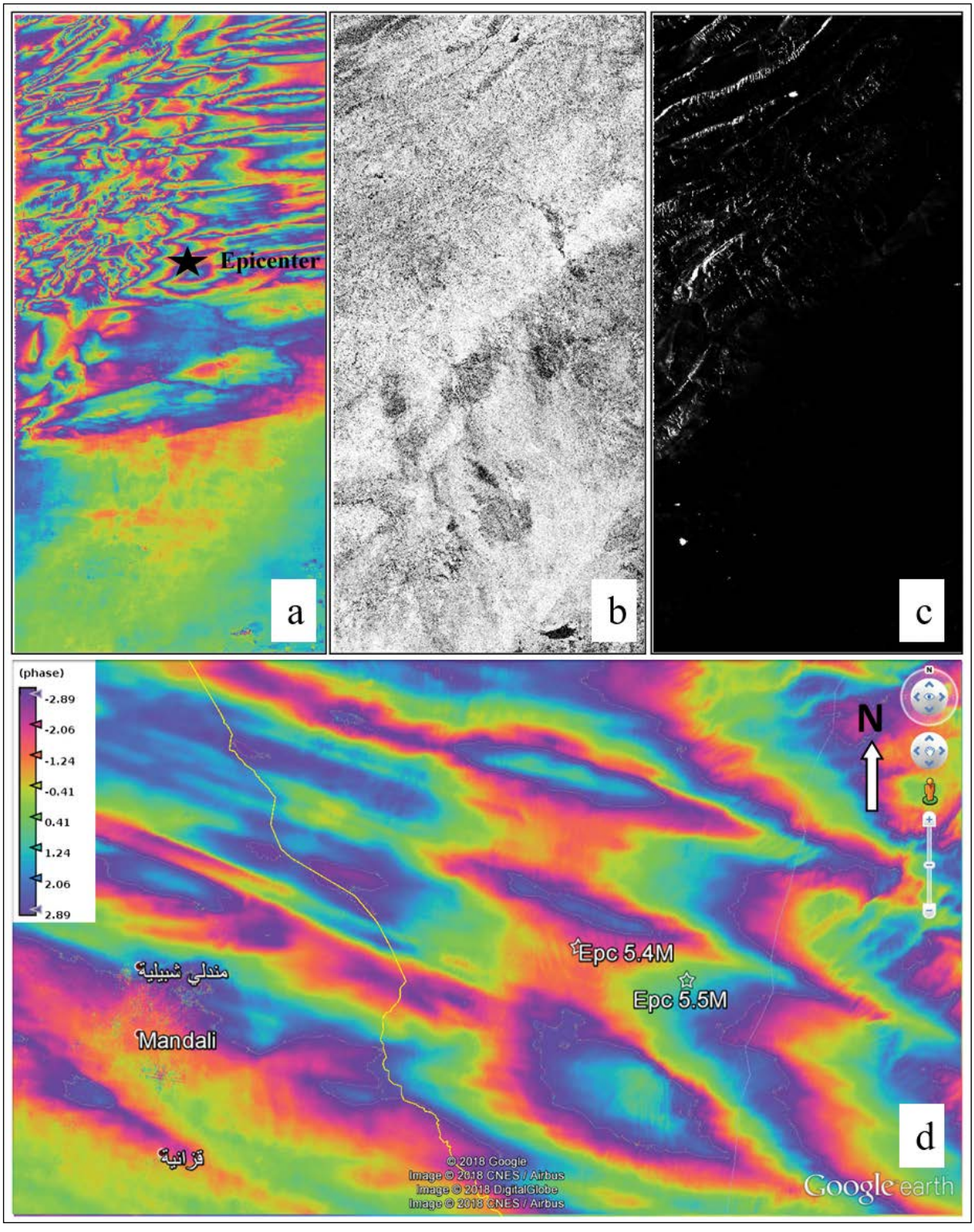

Figure A4- Interferograms from Sentinel-1 InSAR pairs (31 December 2017 - 12 January 2018 06 VV - DESCENDING), a) interferogram, b) intensitiy, c) coherence maps and d) filtered interferogram. There is no information about displacement due to weather conditions.

04 January 2018 - 16 January 2018 72 VV - ASCENDING

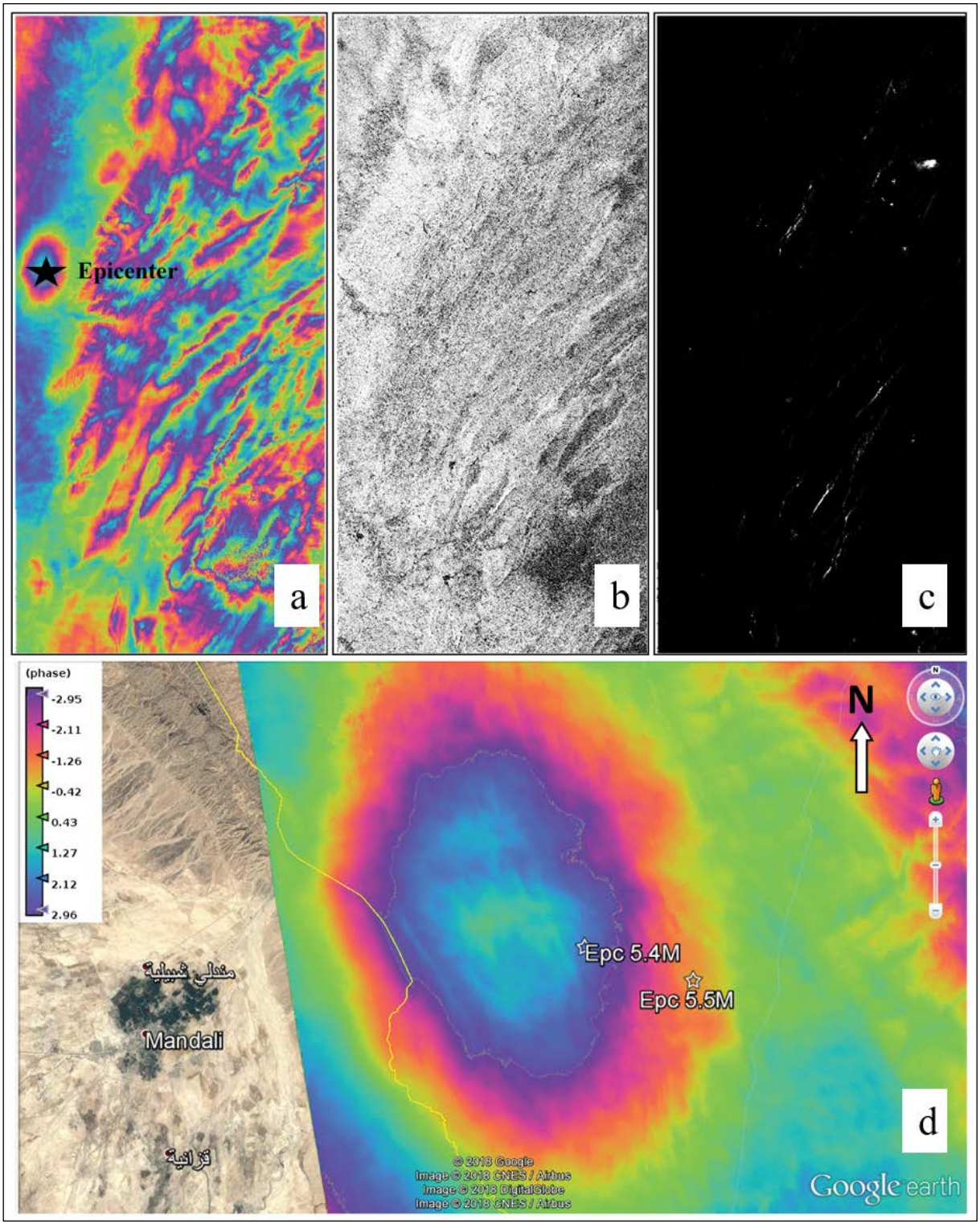

Figure A5- Interferograms from Sentinel-1 InSAR pairs (04 January 2018 - 16 January 2018 72 VV - ASCENDING), a) interferogram, b) intensitiy, c) coherence maps and d) filtered interferogram. Each fringe is colored by the cycle of $-\pi$ to π.